Article

Neuron

Inhibitory Gating of Input Comparison in the CA1 Microcircuit

Highlights

- Excitatory and inhibitory input summation in CA1 is nonlinear and frequency-dependent
- CA1 pyramidal cells report coincidence of CA3 and ECIII inputs with complex spikes
- NPY^+ but not PV^+ or SST^+ interneurons in CA1 also integrate both input pathways
- NPY^+ interneurons in CA1 potently inhibit dendritic excitability in pyramidal cells

Authors

Aaron D. Milstein, Erik B. Bloss, Pierre F. Apostolides, Sachin P. Vaidya, Geoffrey A. Dilly, Boris V. Zemelman, Jeffrey C. Magee

Correspondence

mageej@janelia.hhmi.org

In Brief

CA3 and ECIII inputs to CA1 target distinct dendritic domains of pyramidal cells and recruit specific classes of interneurons. Milstein et al. quantify contributions by short-term plasticity, dendritic amplification, and compartmentalized inhibition to synaptic filtering dynamics during dual pathway integration.

Milstein et al., 2015, Neuron *87*, 1274–1289
September 23, 2015
http://dx.doi.org/10.1016/j.neuron.2015.08.025

CellPress

CellPress

Neuron
Article

Inhibitory Gating of Input Comparison in the CA1 Microcircuit

Aaron D. Milstein,[1] Erik B. Bloss,[1] Pierre F. Apostolides,[1] Sachin P. Vaidya,[1] Geoffrey A. Dilly,[2] Boris V. Zemelman,[2] and Jeffrey C. Magee[1,*]
[1]Howard Hughes Medical Institute, Janelia Research Campus, Ashburn, VA 20147, USA
[2]Center for Learning and Memory, University of Texas at Austin, Austin, TX 78712, USA
*Correspondence: mageej@janelia.hhmi.org
http://dx.doi.org/10.1016/j.neuron.2015.08.025

SUMMARY

Spatial and temporal features of synaptic inputs engage integration mechanisms on multiple scales, including presynaptic release sites, postsynaptic dendrites, and networks of inhibitory interneurons. Here we investigate how these mechanisms cooperate to filter synaptic input in hippocampal area CA1. Dendritic recordings from CA1 pyramidal neurons reveal that proximal inputs from CA3 as well as distal inputs from entorhinal cortex layer III (ECIII) sum sublinearly or linearly at low firing rates due to feedforward inhibition, but sum supralinearly at high firing rates due to synaptic facilitation, producing a high-pass filter. However, during ECIII and CA3 input comparison, supralinear dendritic integration is dynamically balanced by feedforward and feedback inhibition, resulting in suppression of dendritic complex spiking. We find that a particular subpopulation of CA1 interneurons expressing neuropeptide Y (NPY) contributes prominently to this dynamic filter by integrating both ECIII and CA3 input pathways and potently inhibiting CA1 pyramidal neuron dendrites.

INTRODUCTION

The central nervous system processes sensory information through many layers of neuronal circuitry, ultimately producing signals that drive behaviors appropriate to the demands of the environment. The signal transformations, or computations, that occur at each stage of processing in the brain emerge from the morphological and biophysical properties of the neurons involved (Johnston et al., 1996; Magee, 2000; London and Häusser, 2005; Spruston, 2008), their anatomical and functional connectivity (Bock et al., 2011; Briggman et al., 2011; Bargmann and Marder, 2013), and their temporal dynamics (Abbott and Regehr, 2004; George et al., 2011; Womelsdorf et al., 2014). It is well-known that specific features of the sensory environment and the behavior of an animal can be decoded from the rate and timing of action potentials in neurons that process those features (deCharms and Zador, 2000; Ahmed and Mehta, 2009). However, the cellular and circuit mechanisms that integrate and filter synaptic inputs to generate such receptive fields remain poorly understood. In this study we focus on hippocampal area CA1 as a model system for understanding how neuronal circuits selectively respond to specific spatial and temporal patterns of synaptic inputs.

The mammalian hippocampus processes and stores information about the topology of spatial environments and the order of events in time (O'Keefe, 1979; Buzsáki and Moser, 2013; Eichenbaum, 2013). The firing patterns of CA1 pyramidal neurons encode the position of an animal in physical space during navigation, hence they are referred to as "place cells," and their spatial receptive fields as "place fields" (O'Keefe, 1979). The local neuronal circuit in area CA1 that computes these distinctive receptive fields shares prominent features with many circuits throughout the brain (Grillner et al., 2005; Silberberg et al., 2005; Womelsdorf et al., 2014), despite differences in the sources and content of the signals they process:

(1) Multiple input pathways of distinct origin target different dendritic compartments of the output neurons (Petreanu et al., 2009; Larkum, 2013). In CA1, it is an intrahippocampal input from area CA3 that contacts basal and proximal apical dendrites of pyramidal cells and an external cortical input from ECIII that contacts distal apical tuft dendrites (Witter, 1993; Kajiwara et al., 2008; Takahashi and Magee, 2009).
(2) Those pathways differentially activate multiple classes of local inhibitory interneurons that also target specific domains (Somogyi and Klausberger, 2005; Kajiwara et al., 2008; Takács et al., 2012; Somogyi et al., 2014). In this study we investigate three genetically defined interneuron subtypes, expressing either parvalbumin (PV), neuropeptide Y (NPY), or somatostatin (SST), that respectively innervate the perisomatic region, the apical dendrites, and the distal tuft dendrites of CA1 pyramidal cells.
(3) Presynaptic neurotransmitter release at each input pathway is stochastic, use-dependent, and target-selective (Markram et al., 1998; Reyes et al., 1998; Losonczy et al., 2002; Wierenga and Wadman, 2003; Mori et al., 2004; Pouille and Scanziani, 2004; Richardson et al., 2005; Sun et al., 2005; Klyachko and Stevens, 2006). For example, it has been shown that synapses from CA3 onto CA1 pyramidal cells exhibit an initially low release probability (P_r) that robustly facilitates during

bouts of repetitive firing, whereas synapses from the same CA3 axons onto some CA1 interneurons have an initially higher P_r that moderately facilitates or even depresses during a train (Wierenga and Wadman, 2003; Sun et al., 2005).

(4) The cable properties of branching dendrites and their expression of voltage-dependent ion channels can either attenuate or amplify synaptic signals (Johnston et al., 1996; Magee, 2000; Spruston, 2008), expanding the diversity of neuronal circuit computations (London and Häusser, 2005).

(5) The resulting output signals reflect comparisons made between the multiple input pathways (Larkum et al., 1999; Spruston, 2008; Takahashi and Magee, 2009; Xu et al., 2012; Larkum, 2013), as well as a dynamic balance of excitation and inhibition (Pouille and Scanziani, 2004; Haider et al., 2006; Klyachko and Stevens, 2006; George et al., 2011; Isaacson and Scanziani, 2011).

One feature of CA1 that is more atypical is its lack of appreciable excitatory feedback (Knowles and Schwartzkroin, 1981), which presents an experimental advantage for measuring the input-output transformation performed by a single neuronal circuit layer. In order to determine the contributions of various network components to information processing within the CA1 microcircuit, we performed intracellular recordings from pyramidal neuron dendrites and interneuron cell bodies in hippocampal slices combined with electrical and optogenetic stimulation. We found that pyramidal neurons select for bursts of synaptic inputs that engage supralinear integration mechanisms and overcome initial barriers of release probability and feedforward inhibition. However, we also observed multiple classes of CA1 interneurons to summate synaptic inputs supralinearly. In particular, we identified a subpopulation of NPY^+ interneurons at the border of the CA3 and ECIII input layers that perform a similar dual pathway coincidence detection operation as pyramidal cells, effectively predicting and preventing complex spike output from CA1.

RESULTS

Frequency-Dependent Input Summation in CA1 Pyramidal Cells and Interneurons

We measured temporal summation of synaptic inputs in each of four cell types in the CA1 microcircuit at the two major input pathways to CA1 (proximal input from CA3 and distal input from ECIII, see diagrams in Figure 1). We observed that triplets of excitatory postsynaptic potentials (EPSPs) do not summate when evoked at 300 ms intervals by electrical stimulation of afferent axons. If P_r at these synapses were static, and postsynaptic integration mechanisms were linear, then EPSPs elicited closer together in time would sum exactly linearly (these expected EPSP amplitudes for varying inter-stimulus intervals (ISIs) are depicted in blue in Figure 1). In the absence of inhibition, any divergence from this expected linear sum in the actual measured response (black in Figure 1) could result from use-dependent changes in P_r (Markram et al., 1998) as well as postsynaptic amplification or attenuation by various voltage-dependent ion channels, including AMPARs, NMDARs, Na^+-, Ca^{2+}-, K^+-, and HCN-channels (Johnston et al., 1996; Magee, 2000; Losonczy and Magee, 2006; Spruston, 2008; Takahashi and Magee, 2009; Grienberger et al., 2014). The combined influences of these diverse integration mechanisms comprise the "excitatory synaptic filter." In the presence of inhibition, diverse mechanisms could contribute to any reduction in measured summation (red in Figure 1), including changes in P_r at excitatory synapses onto inhibitory neurons, postsynaptic integration mechanisms within inhibitory neurons, changes in P_r at inhibitory synapses, effects of inhibition on dendritic excitability, and inhibitory interactions among interneurons (Mori et al., 2004; Pouille and Scanziani, 2004; Richardson et al., 2005; Klyachko and Stevens, 2006; George et al., 2011; Lovett-Barron et al., 2012; Palmer et al., 2012; Pfeffer et al., 2013). These mechanisms comprise the "inhibitory synaptic filter." Here we quantify the frequency dependence of these filters.

We found with intracellular recordings from apical trunk dendrites at the border of strata radiatum (SR) and lacunosum-moleculare (SLM) that pyramidal cells respond to both ECIII and CA3 inputs with facilitating excitation (Figures 1A–1C). While summation was reduced by inhibition, significant supralinearity persisted for ECIII inputs activated at 100 Hz (10 ms ISI) and for CA3 inputs activated at 20 Hz or greater ($\leq$50 ms ISI), generating a high-pass filter (Figures 1A–1C). Next we targeted recordings to genetically labeled somata of PV^+ inhibitory interneurons in strata pyramidale (SP) and oriens (SO) (see Figures 1D, S1, and S2 and Experimental Procedures) and found that they respond weakly to ECIII input (likely through excitatory feedback from CA1 pyramidal neurons) but respond robustly to CA3 input with facilitating excitation (Figures 1E and 1F). While previous studies have reported CA1 basket cells to receive depressing feedback inputs from CA1 pyramidal cells (Losonczy et al., 2002; Pouille and Scanziani, 2004), other work corroborates our observation of facilitation at feedforward inputs from CA3 (Wierenga and Wadman, 2003), which was likely favored by our use of more physiological levels of extracellular Ca^{2+} (Jones and Keep, 1988). However, we found that inhibition onto PV^+ cells reduces summation such that responses are supralinear only for low-input frequencies (10 and 20 Hz, or 100 and 50 ms ISIs), generating a low-pass filter (Figures 1E and 1F).

Recordings from NPY^+ interneuron somata at the border of SR and SLM (see Figures 1G, S1, and S2 and Experimental Procedures) revealed facilitating excitation at both ECIII and CA3 inputs (Figures 1H and 1I). In the presence of inhibition, ECIII inputs exhibited supralinear summation for intermediate input frequencies (10 and 40 Hz, or 100 ms and 25 ms ISIs), as did CA3 inputs for all input frequencies 10 Hz and greater, generating a band-pass filter (Figures 1H and 1I). SST+ somata in stratum oriens (SO) (see Figures 1J, S1, and S2 and Experimental Procedures) responded weakly to ECIII input stimulation and only responded to CA3 input stimulation when inhibition was blocked, and after a delay (Figures 1K and 1L), consistent with previous reports that oriens lacunosum-moleculare (O-LM) neurons lack direct inputs from ECIII and CA3 (Maccaferri and McBain, 1995; Kim et al., 2012) but receive a facilitating feedback connection from CA1 pyramidal cells (Ali and Thomson, 1998; Losonczy et al., 2002).

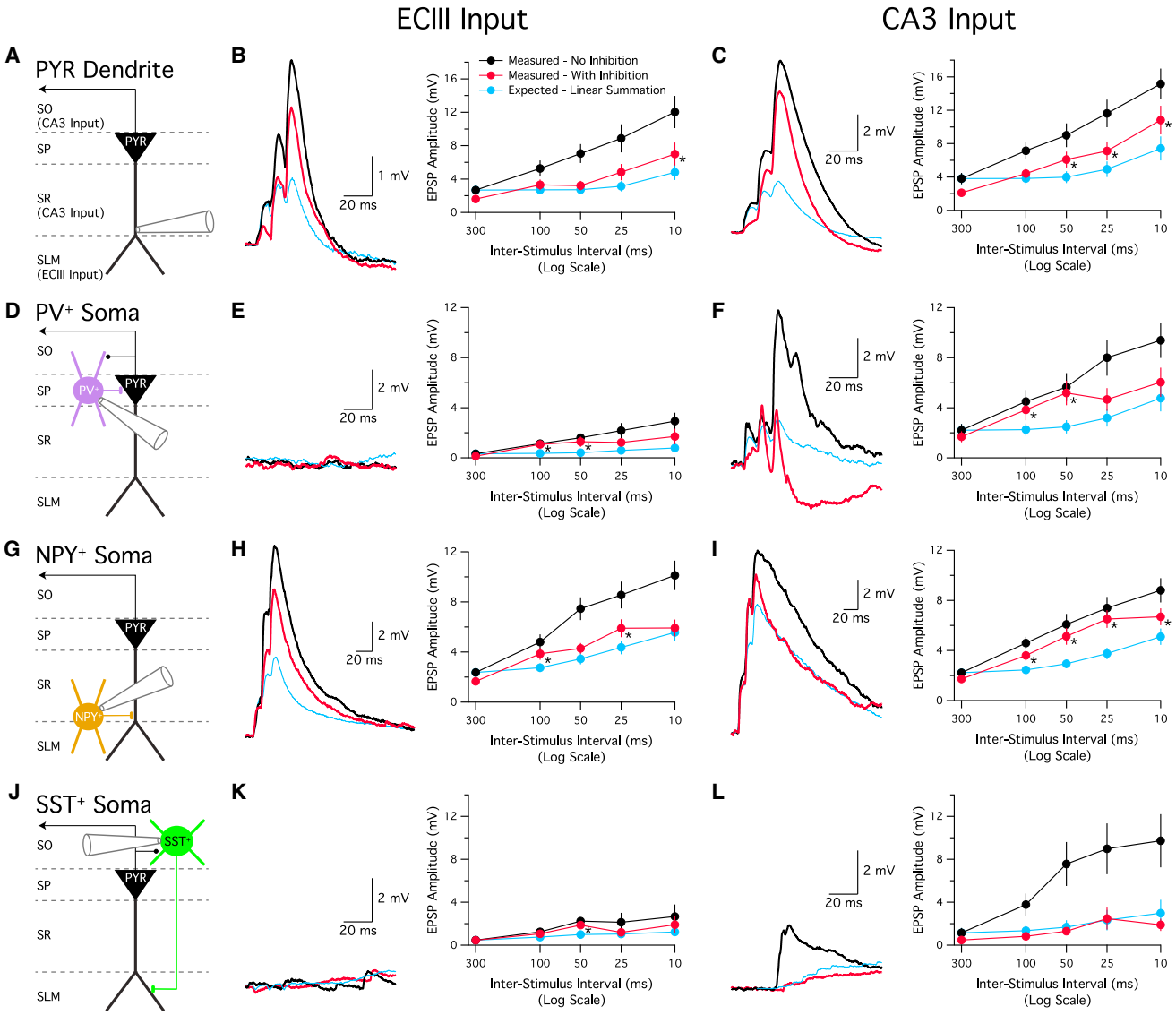

Figure 1. Nonlinear Summation in CA1 Depends on Input Pathway, Input Frequency, and Cell Type

(A) Schematic indicating recording position from the distal apical trunk dendrite of a CA1 pyramidal neuron near the border of SR and SLM (~300 μm from the cell body) during electrical stimulation of CA3 axons in SR and ECIII axons in SLM.

(B) Synaptic inputs from ECIII were stimulated across a range of inter-stimulus intervals (ISI) in the presence and absence of GABAergic inhibition. The average EPSP recorded at 300 ms ISI without inhibition was used to calculate the expected EPSP waveform for other ISIs, assuming linear summation. Left: example traces compare the expected (blue) EPSP waveform to the measured voltage responses with (red) and without (black) inhibition for inputs evoked at 10 ms ISI. Right: summary data from these experiments display peak EPSP amplitude as mean ± SEM for each ISI (n = 15). Asterisks denote a significant difference ($p < 0.05$) between the measured EPSP with inhibition (red) and the expected EPSP (blue). Unless otherwise indicated below, in all subsequent panels the measured EPSP amplitude without inhibition (black) also differed significantly ($p < 0.05$) from the other two conditions at all ISIs, except for 300 ms, when the expected EPSP is by definition equal to the measured EPSP without inhibition.

(C) Same as in (B) for synaptic inputs from CA3. EPSPs evoked by stimulation in either proximal SR or distal SR were pooled (n = 19).

(D–F) Same as in (A)–(C) for recordings from the cell bodies of PV^+ interneurons in SP and SO. (E) n = 9. (F) n = 18. The measured EPSP without inhibition only differed significantly ($p < 0.05$) from that with inhibition at ISIs of 300 ms, 25 ms, and 10 ms in both (E) and (F).

(G–I) Same as in (A)–(C) for recordings from the cell bodies of NPY^+ interneurons at the border of SR and SLM. (H) n = 20. (I) n = 35. The measured EPSP without inhibition only differed significantly ($p < 0.05$) from that with inhibition at ISIs of 300 ms, 100 ms, and 10 ms in (I).

(J–L) Same as in (A)–(C) for recordings from the cell bodies of SST^+ interneurons in SO. (K) The measured EPSP without inhibition did not differ significantly from that with inhibition at any ISI in (K), and only differed from the expected EPSP at 50 ms ISI (n = 4–5). (L) n = 8–14.

See also Figures S1 and S2.

Synaptic Filter Dynamics in CA1 Pyramidal Neurons during Dual Pathway Integration

The above observations suggest that the CA1 microcircuit acts as a high-pass filter, favoring excitation over inhibition in pyramidal cells when synaptic inputs from either ECIII or CA3 are activated repeatedly at high frequency. They also identify NPY^+ cells at the border of SR and SLM as a unique class of interneurons that send dendrites into both layers (Figure S2) and are capable of summating both input pathways supralinearly. We therefore wondered how the excitatory and inhibitory synaptic filters in CA1 evolve when both ECIII and CA3 inputs are coactive, as occurs in vivo during spatial exploration (Buzsáki, 2002; Ahmed and Mehta, 2009; Mizuseki et al., 2009; Buzsáki and Moser, 2013; Schomburg et al., 2014). Previous work has demonstrated that, in the absence of inhibition, synchronous activity across both input pathways recruits dendritic amplification mechanisms to generate complex spikes in CA1 pyramidal cells, which are characterized by long-duration plateau potentials in the apical trunk and high-frequency action potentials riding on a large slow depolarization at the soma (Takahashi and Magee, 2009). However, it is unclear how the local inhibitory microcircuit influences dual pathway integration.

We chose a spatially and temporally patterned stimulus to mimic the timing and rhythmicity of synaptic inputs to CA1 place cells in vivo during place field traversal (Buzsáki, 2002; Buzsáki and Moser, 2013). Previous work has demonstrated that active ensembles of ECIII and CA3 neurons fire in punctuated bursts in sync with the oscillating extracellular local field potential (LFP) in CA1 (Buzsáki, 2002; Ahmed and Mehta, 2009; Buzsáki and Moser, 2013), with ECIII inputs exerting their peak influence in CA1 near the start (or peak) of each theta cycle, followed by CA3 inputs after a brief phase delay (Mizuseki et al., 2009; Schomburg et al., 2014). For five simulated theta cycles with duration 150 ms each, bursts of five stimuli were delivered at 100 Hz either to one electrode in SLM to activate ECIII inputs, to two electrodes in SR to activate both proximal and distal CA3 inputs, or all three electrodes simultaneously, with ECIII stimuli preceding CA3 stimuli by 15 ms (schematized in Figures 2, 3, 4, 5, and 6).

Recordings from CA1 pyramidal neuron apical trunk dendrites revealed striking dynamics in excitatory and inhibitory synaptic filtering, both within and across theta cycles (Figures 2 and 3). Under all stimulation conditions, pharmacologically blocking inhibition increased spike rate and advanced the phase of spike onset (Figures 2A, 2C, 2D, 4D, and 4E), consistent with the presence of fast, early-onset feedforward inhibition that influences the rate and timing of pyramidal cell firing (Pouille and Scanziani, 2001; Losonczy et al., 2010; Royer et al., 2012). When multiple spikes occurred within a theta cycle, spike amplitudes decreased and spike rise kinetics slowed throughout the train, particularly during complex spike bursts (Figure S3). We validated that spikes detected in the apical trunk dendrite under these conditions accurately reflect somatic output by simultaneously recording from the soma and apical trunk in a separate group of cells (Figure S3) (see also Magee and Johnston, 1997; Takahashi and Magee, 2009).

In order to quantify the degree of supralinear summation resulting from both presynaptic release dynamics and postsynaptic dendritic excitability during theta burst stimulation, and to permit comparison across stimulation pathway conditions with and without inhibition, we performed a similar analysis of measured versus expected depolarization to that shown in Figure 1 (see Experimental Procedures for details). Expected waveforms of depolarization computed from the linear sum of averaged single pulse responses to stimulation of individual input pathways without inhibition are shown for reference in blue in Figures 2A and 2B. The differences between measured and expected waveforms of depolarization are shown in Figures 3A and 3B. Within each theta cycle, excitatory inputs summated supralinearly, overcoming early phase inhibition and recruiting pyramidal cells to spike (Figures 2A, 2C, 3A, and 3C). However, a late phase inhibitory component reduced dendritic integration and prevented simple spikes from progressing to long duration complex spikes (Figures 2A, 2E, 3A, 3C, and 3D). Across theta cycles, facilitating excitation increased supralinear summation (Figure 3C), firing rate (Figure 2C), and spike width (Figure 2E). This facilitation within and across theta cycles allowed punctuated bursts of ECIII inputs to overcome substantial distance-dependent attenuation and to drive some CA1 cells to spike in the absence of CA3 input (Figures 2A and 2C), consistent with reports that ECIII inputs are sufficient to drive CA1 place cell firing in vivo (Brun et al., 2002; Nakashiba et al., 2008). Contrary to previous work that employed different recording and stimulation configurations (Ang et al., 2005; Chevaleyre and Siegelbaum, 2010) (see Supplemental Experimental Procedures and Figure S7), we did not find ECIII inputs to be subject to a more potent inhibitory filter than CA3 inputs (Figures 2A, 2C, 3A, 3C, and 6B). Dendritic plateau potentials driving complex spike bursts were only observed when ECIII and CA3 input pathways were synchronously activated in the complete absence of inhibition and reached their longest duration after multiple theta cycles (Figures 2A, 2E, 3A, and 3C) (Takahashi and Magee, 2009). However, inhibition completely prevented these regenerative dendritic events.

We next tested the role of presynaptic P_r and short-term dynamics in shaping the excitatory and inhibitory synaptic filters by increasing the extracellular Ca^{2+} concentration from near physiological 1.3 mM to 2.5 mM (Jones and Keep, 1988; Murthy et al., 1997). While this manipulation increased the response to single pulse stimulation of CA3 inputs, as expected from an increase in basal release probability (Figure S4), it converted changes in summation across theta cycles in pyramidal cells from facilitating to depressing (Figures 2B, 2C, 3B, 3C, and S4). It decreased the magnitude and advanced the phase of supralinear summation (Figures 3B–3D), reduced the duration of complex spikes induced by coactivation of ECIII and CA3 inputs in the absence of inhibition (Figures 2B and 2E), and completely prevented the ability of high-frequency inputs to induce spiking in the presence of inhibition (Figures 2B and 2C). Taken together, these results show that use-dependent and target-selective changes in release probability, postsynaptic amplification in dendrites, and multiple phasic components of inhibition all contribute to temporally dynamic nonlinear filtering of synaptic input in CA1 pyramidal cells.

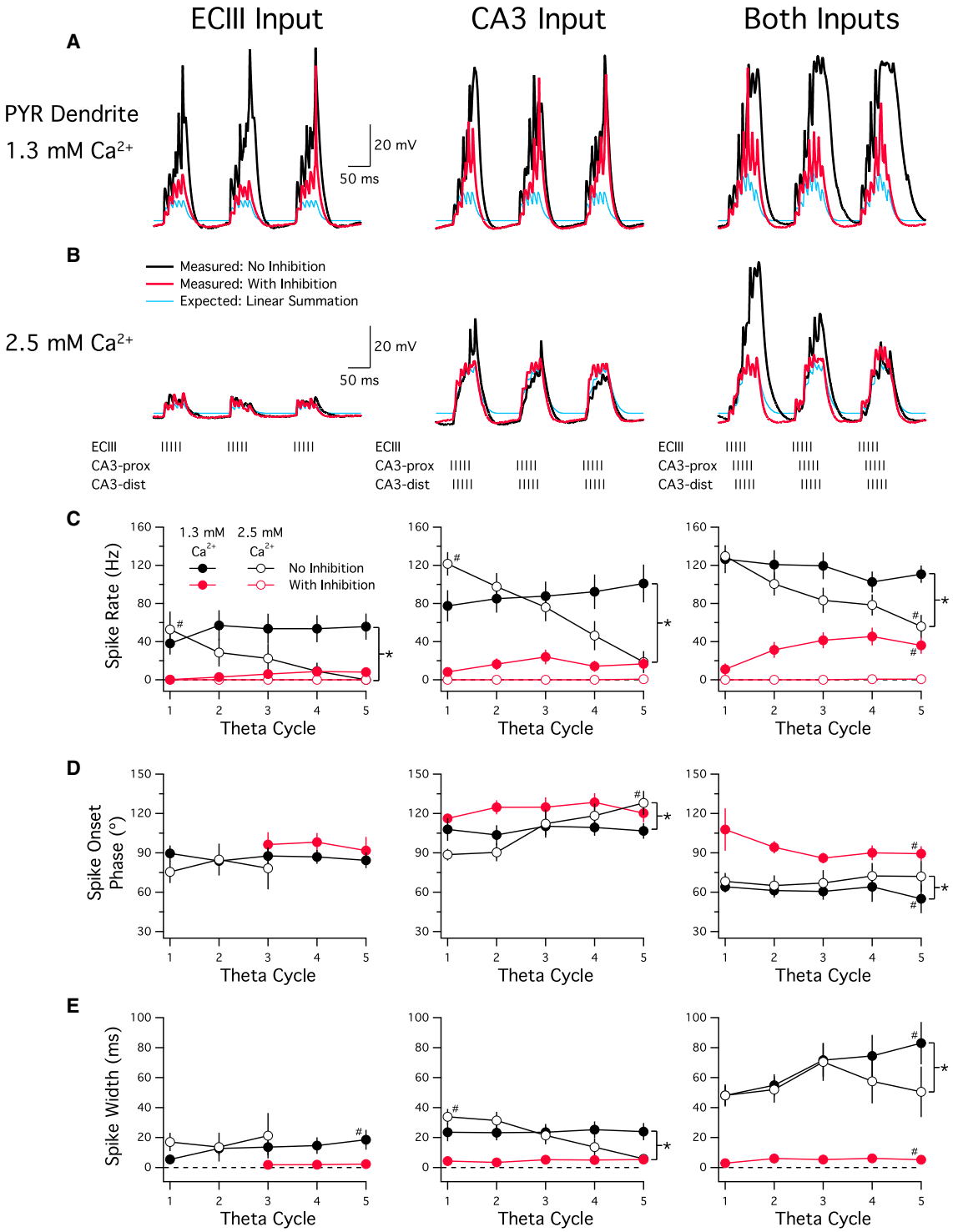

Figure 2. Excitatory and Inhibitory Filter Dynamics Regulate CA1 Pyramidal Cell Spike Output

(A) Example traces of a distal dendritic recording from a CA1 pyramidal neuron during theta burst stimulation, schematized below in (B). Responses to the last 3/5 theta cycles of stimulation are shown for ECIII inputs alone (left), CA3 inputs alone (center), and both inputs together (right). The expected EPSP waveforms (blue), calculated as the linear sum of the averaged responses to single pulse stimulation of individual pathways without inhibition, as in Figure 1 (see Experimental Procedures), are compared to the measured voltage responses with (red) and without (black) inhibition. Long duration dendritic complex spikes were observed when ECIII and CA3 inputs were coactivated in the absence of inhibition.

(legend continued on next page)

Coincidence Detection of ECIII and CA3 Inputs in CA1 Interneurons

In order to determine the contributions of various CA1 interneuron subtypes to the dynamic inhibitory filter measured in pyramidal cells, we next performed somatic recordings from genetically labeled interneurons (Figure S2) using the same dual pathway theta stimulation protocol described above. We found that, in response to CA3 inputs, PV^+ interneurons in SP and SO exhibited facilitation followed by depression (Figures 5A and 5D), initiated spikes significantly earlier than pyramidal cells (Figure 4E), and maintained high firing rates throughout stimulation (Figures 4A and 4D), but were not driven to spike by ECIII inputs alone (Figures 4A and 4D). Surprisingly, PV^+ interneurons did not further increase their firing rate during dual pathway stimulation relative to CA3 alone (Figures 4A and 4D), despite receiving feedback inputs from CA1 pyramidal cells, which were most active during ECIII and CA3 coactivation (Figures 2A, 2C, and 4D). This was not due to saturation of firing rate by CA3 feedforward inputs under these conditions because PV^+ cells increased their firing rates upon pharmacologically blocking inhibition (Figure S5). Rather, it is possible that feedback inhibition as well as presynaptic depression at CA1 excitatory feedback inputs to PV^+ cells limits their efficacy. Consistent with the presence of both late phase excitation and inhibition resulting from pyramidal cell output, supralinear summation in PV^+ cells was reduced in magnitude and slightly delayed in phase during dual pathway stimulation compared to CA3 alone (Figures 5A, 5D, and 5E).

In contrast, NPY^+ interneurons at the border of SR and SLM were driven to spike by either ECIII or CA3 inputs alone, and further increased their firing rate during coincident stimulation of both pathways (Figures 4B and 4D), resembling pyramidal neurons. While supralinear summation of ECIII inputs in NPY^+ cells was reduced in magnitude and resulting spiking was delayed in phase compared to pyramidal cells (Figures 4B, 4E, 5B, 5D, and 5E), CA3 inputs facilitated more rapidly and robustly (Figures 5B, 5D, and 5E), causing NPY^+ cells to spike significantly earlier in phase than pyramidal cells (Figures 4B and 4E). NPY^+ cells also responded to coincidence of ECIII and CA3 inputs by further advancing the phase of spike onset (Figures 4B and 4E).

SST^+ O-LM interneurons integrated inputs later in phase than any other cell type (Figures 5C and 5E), consistent with their role as an exclusively feedback-inhibitory component of the circuit (Maccaferri and McBain, 1995; Kim et al., 2012). While ECIII and CA3 input coactivation slightly advanced the phase of summation (Figures 5C and 5E) and spike onset (Figures 4C and 4E) compared to CA3 alone, the spike rate of SST^+ cells was not significantly modulated (Figures 4C and 4D).

Dynamic Imbalance of Excitation and Inhibition in CA1

The above results clearly show that various components of the excitatory and inhibitory synaptic filters in the CA1 microcircuit are temporally dynamic. Each cell type integrates patterned activity at each input pathway differently and responds with a preferred rate and phase of firing. In order to further quantify this temporally dynamic interplay between excitation and inhibition and compare across cell types, we defined a continuously varying metric, "E:I Imbalance," that captures the relative contributions of excitation and inhibition to EPSP amplitude (see Experimental Procedures). This metric is valued at 0.5 when the entire excitatory response is completely cancelled by precisely balanced inhibition and is valued at 1 when blocking inhibition has no effect on EPSP amplitude. Figure 6A displays the average E:I Imbalance waveforms for each cell type recorded during coactivation of both ECIII and CA3 input pathways. In pyramidal neuron dendrites, E:I Imbalance rapidly increased (in favor of excitation) at the start of each theta cycle of stimulation, as repetitive input activation facilitated excitation and depressed early phase feedforward inhibition (Figure 6A) (Mori et al., 2004; Pouille and Scanziani, 2004; Klyachko and Stevens, 2006). However, before the end of stimulation and postsynaptic integration, E:I Imbalance rapidly decreased (in favor of inhibition), reflecting increasing contributions by late phase feedforward and feedback inhibition (Figure 6A) (Pouille and Scanziani, 2004). Excitation and inhibition also fluctuated in and out of balance to varying degrees and with distinct time courses in each of the recorded interneuron subtypes (Figures 6A–6C). All three interneuron subtypes remained out of balance later in phase than pyramidal neurons (Figure 6C), consistent with their contributing to the late phase inhibition received by pyramidal neurons. Interestingly, NPY^+ interneurons at the SR/SLM border were less modulated by inhibition than any other cell type recorded (Figure 6B). These results underscore that spatiotemporally correlated input patterns transiently disrupt the balance between excitation and inhibition within neuronal microcircuits, which is expected to contribute to the selectivity of neuronal receptive fields (Richardson et al., 2005; Haider et al., 2006; Isaacson and Scanziani, 2011; but see Atallah and Scanziani, 2009; Xue et al., 2014).

Functional Impact of CA1 Interneuron Subtypes on Dendritic Excitability

Of the three interneuron cell types characterized above, NPY^+ "border" interneurons exhibited spatial and temporal summation of synaptic inputs that was most similar to pyramidal neurons, positioning this interneuron subtype as a strong candidate to regulate nonlinear pathway interactions in pyramidal cells.

(B) Same as in (A) except extracellular Ca^{2+} concentration was increased from near-physiological 1.3 mM to 2.5 mM to alter release probability (P_r) and short-term synaptic dynamics. Facilitation across cycles and complex spikes were reduced.

(C) The mean spike rate per theta cycle, averaged across cells, is displayed as mean ± SEM for each stimulation and recording condition. Asterisks denote a significant difference ($p < 0.05$) in slope across theta cycles between 1.3 mM Ca^{2+} (black closed circles, n = 11–37) and 2.5 mM Ca^{2+} (black open circles, n = 11) without inhibition. Hash symbols denote a significant difference ($p < 0.05$) across theta cycles within the indicated stimulation and recording condition.

(D) Same as in (C) for the phase of the first spike per theta cycle, averaged across cells (1.3 mM Ca^{2+}: n = 7–19; 2.5 mM Ca^{2+}: n = 5–11). Conditions containing fewer than two spiking cells in a given theta cycle were omitted from quantification for that theta cycle in (D) and (E).

(E) Same as in (D) for the width of the longest duration spike per theta cycle, averaged across cells. Calculated as the full width at half maximum voltage relative to the voltage threshold of the first spike per burst.

See also Figure S3.

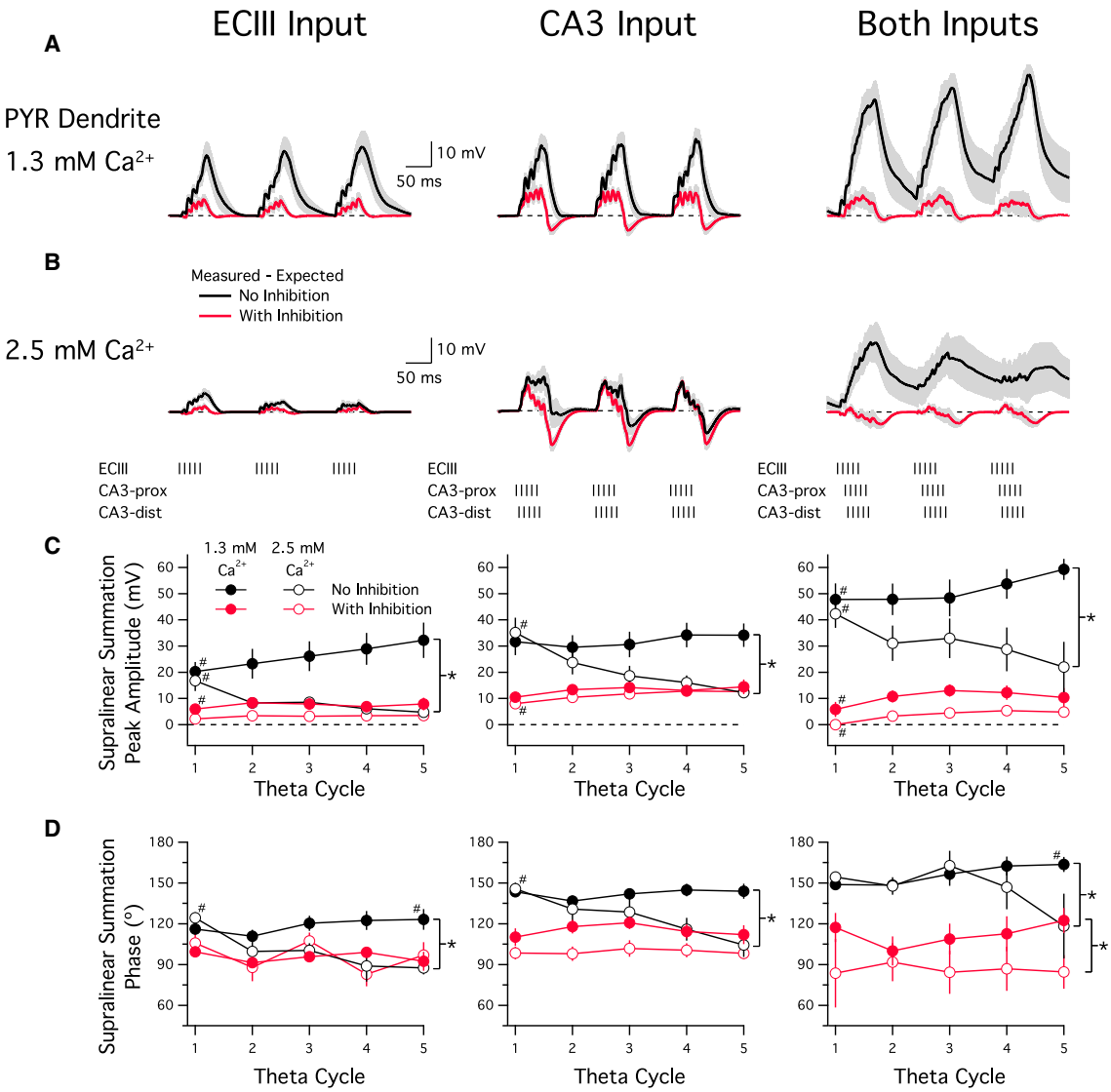

Figure 3. Excitatory and Inhibitory Filter Dynamics Regulate Nonlinear Dendritic Integration in CA1 Pyramidal Cells

(A) Traces from the same stimulation and recording conditions as in Figure 2 were generated by offline removal of fast sodium spikes and hyperpolarizations below resting membrane potential, followed by linear interpolation to isolate the underlying depolarization waveforms. Then the expected EPSP waveforms for each cell, like the examples shown in blue in Figures 2A and 2B, were subtracted from the measured depolarization waveforms from recordings with (red) and without (black) inhibition so that the resulting supralinear (above zero) and sublinear (below zero) components of synaptic summation could be visualized and quantified. In many cells, dendritic depolarization not predicted by the expected linear sum persisted across multiple simulated theta cycles of stimulation without returning to baseline, particularly during long-duration complex spiking. These periods contribute to the quantification of the amplitude and phase of supralinear summation shown here (see Experimental Procedures). Solid lines represent the mean "Measured − Expected" waveforms averaged across cells, and the gray shaded areas represent the SEM across cells.

(B) Same as in (A) except extracellular Ca^{2+} concentration has been increased from near-physiological 1.3 mM to 2.5 mM to alter release probability (P_r) and short-term synaptic dynamics. Supralinear summation was reduced.

(C) The peak amplitude of supralinear summation per theta cycle from the "Measured − Expected" waveforms shown in (A) and (B), averaged across cells, is displayed as mean ± SEM for each stimulation and recording condition. Asterisks denote a significant difference ($p < 0.05$) in slope across theta cycles between 1.3 mM Ca^{2+} (black closed circles, n = 8–13) and 2.5 mM Ca^{2+} (black open circles, n = 9) without inhibition. Hash symbols denote a significant difference ($p < 0.05$) across theta cycles within the indicated stimulation and recording condition.

(D) Same as in (C) for the phase of supralinear summation per theta cycle, averaged across cells. This is calculated from the center of mass of the supralinear component of the "Measured − Expected" waveforms shown in (A) and (B). An additional asterisk in the right panel of (D) indicates a significant difference ($p < 0.05$) in phase between 1.3 mM Ca^{2+} (red closed circles) and 2.5 mM Ca^{2+} (red open circles) with inhibition.

See also Figure S4.

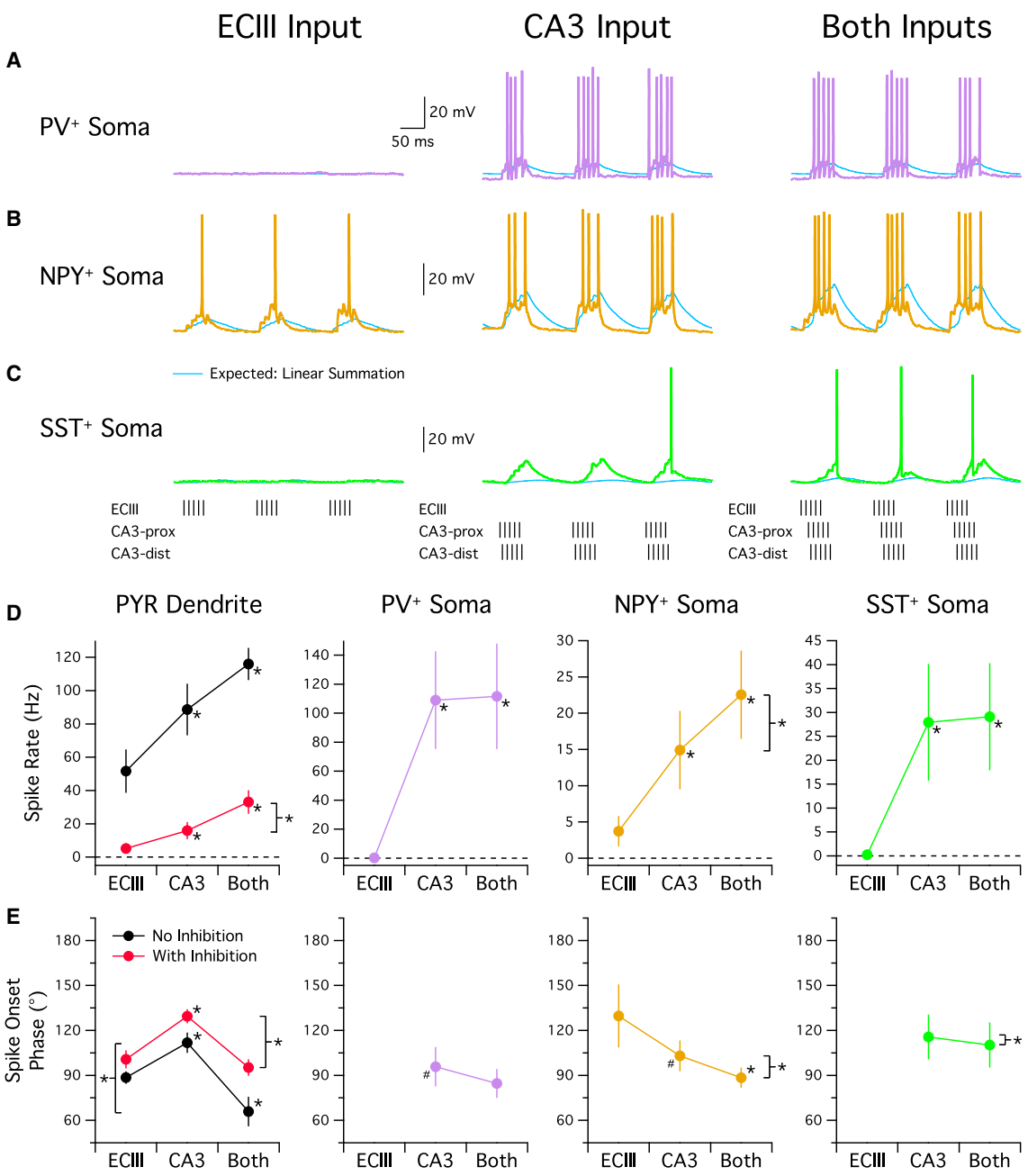

Figure 4. Coincidence Detection of ECIII and CA3 Inputs in CA1 Interneurons

(A–C) Example traces from recordings analogous to those in Figure 2, but from the cell bodies of CA1 interneurons. The expected EPSP waveforms (blue), calculated as in Figures 1 and 2, are compared to the measured voltage responses with intact inhibition. (A) Traces represent recordings from PV^+ interneurons in SP and SO (purple). (B) Traces represent recordings from NPY^+ interneurons at the border of SR and SLM (orange). (C) Traces represent recordings from SST^+ interneurons in SO (green).

(D) The mean spike rate per theta cycle, averaged across theta cycles and cells, is displayed as mean ± SEM for each stimulation condition and neuronal cell type (PYR: n = 11–37; PV^+: n = 10; NPY^+: n = 33–34; SST^+: n = 16). Floating asterisks denote a significant difference ($p < 0.05$) between the indicated pathway stimulation condition and ECIII inputs alone for the indicated cell type. Asterisks next to brackets denote a significant difference ($p < 0.05$) between CA3 inputs alone and both inputs together for the indicated cell type.

(E) Same as in (D) for the phase of the first spike per theta cycle, averaged across theta cycles and cells (PYR: n = 7–18; PV^+: n = 9; NPY^+: n = 10–18; SST^+: n = 6–8). Cell types containing fewer than two spiking cells for a particular pathway stimulation condition were omitted from quantification for that condition. Hash symbols denote a significant difference ($p < 0.05$) between the indicated cell type and pyramidal neurons with inhibition (red) for the indicated pathway stimulation condition.

See also Figures S2 and S5.

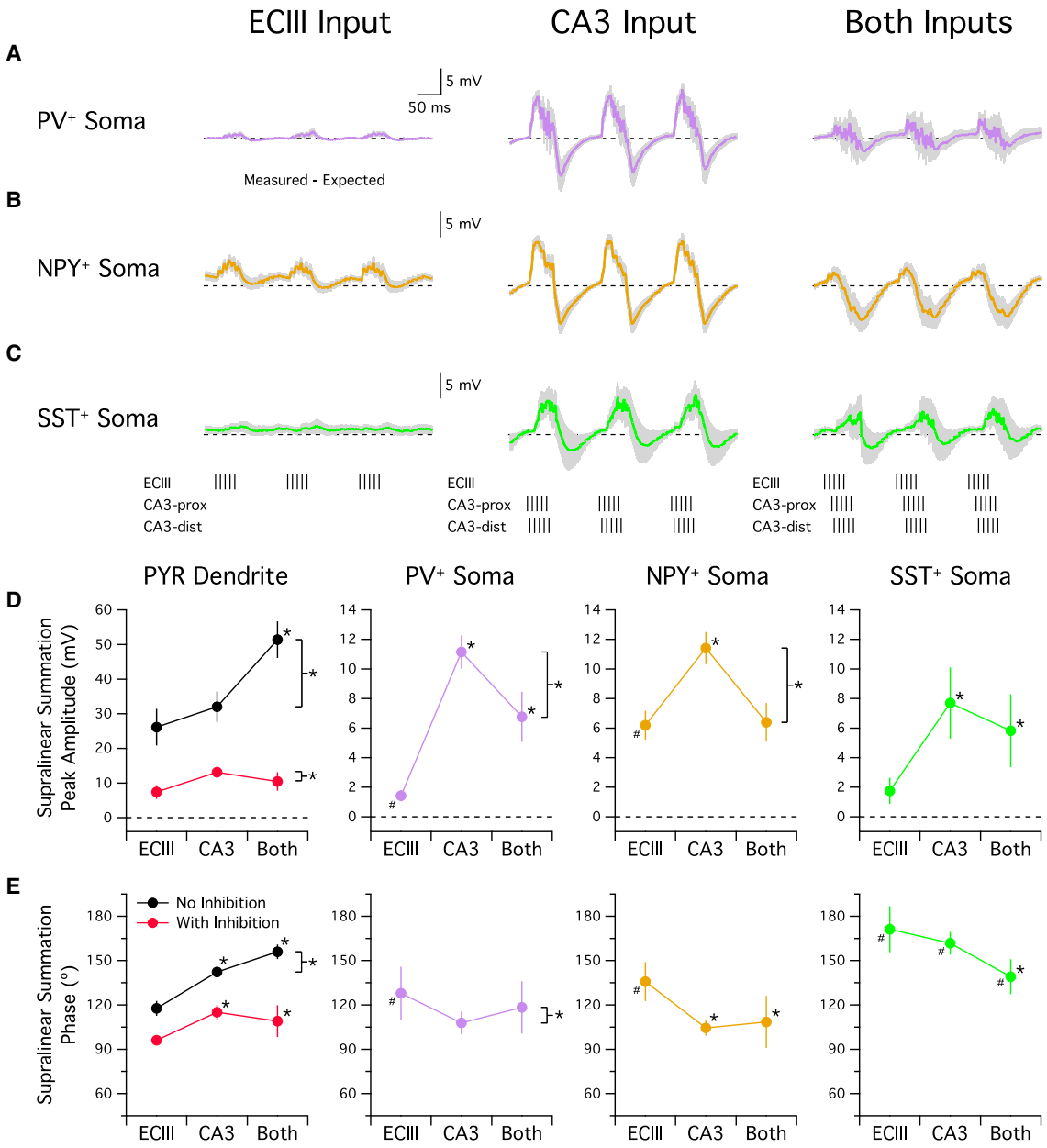

Figure 5. Phasic Nonlinear Summation in CA1 Interneurons

(A–C) "Measured − Expected" traces were calculated using the procedure described in Figure 3 from the same pathway stimulation conditions and cell types as in Figure 4. Solid lines represent the mean "Measured − Expected" waveforms averaged across cells, and the gray shaded areas represent the SEM across cells. (A) Traces represent recordings from PV$^+$ interneurons in SP and SO (purple). (B) Traces represent recordings from NPY$^+$ interneurons at the border of SR and SLM (orange). (C) Traces represent recordings from SST$^+$ interneurons in SO (green).

(D) The peak amplitude of supralinear summation per theta cycle from the "Measured − Expected" waveforms shown in (A)–(C) and Figure 3A, averaged across theta cycles and cells, is displayed as mean ± SEM for each stimulation condition and neuronal cell type (PYR: n = 8–13; PV$^+$: n = 9; NPY$^+$: n = 20–22; SST$^+$: n = 9). Floating asterisks denote a significant difference ($p < 0.05$) between the indicated pathway stimulation condition and ECIII inputs alone for the indicated cell type. Asterisks next to brackets denote a significant difference ($p < 0.05$) between CA3 inputs alone and both inputs together for the indicated cell type. Hash symbols denote a significant difference ($p < 0.05$) between the indicated cell type and pyramidal neurons with inhibition (red) for the indicated pathway stimulation condition.

(E) Same as in (D) for the phase of supralinear summation per theta cycle, averaged across theta cycles and cells. This is calculated from the center of mass of the supralinear component of the "Measured − Expected" waveforms shown in (A)–(C) and Figure 3A.

See also Figures S2 and S5.

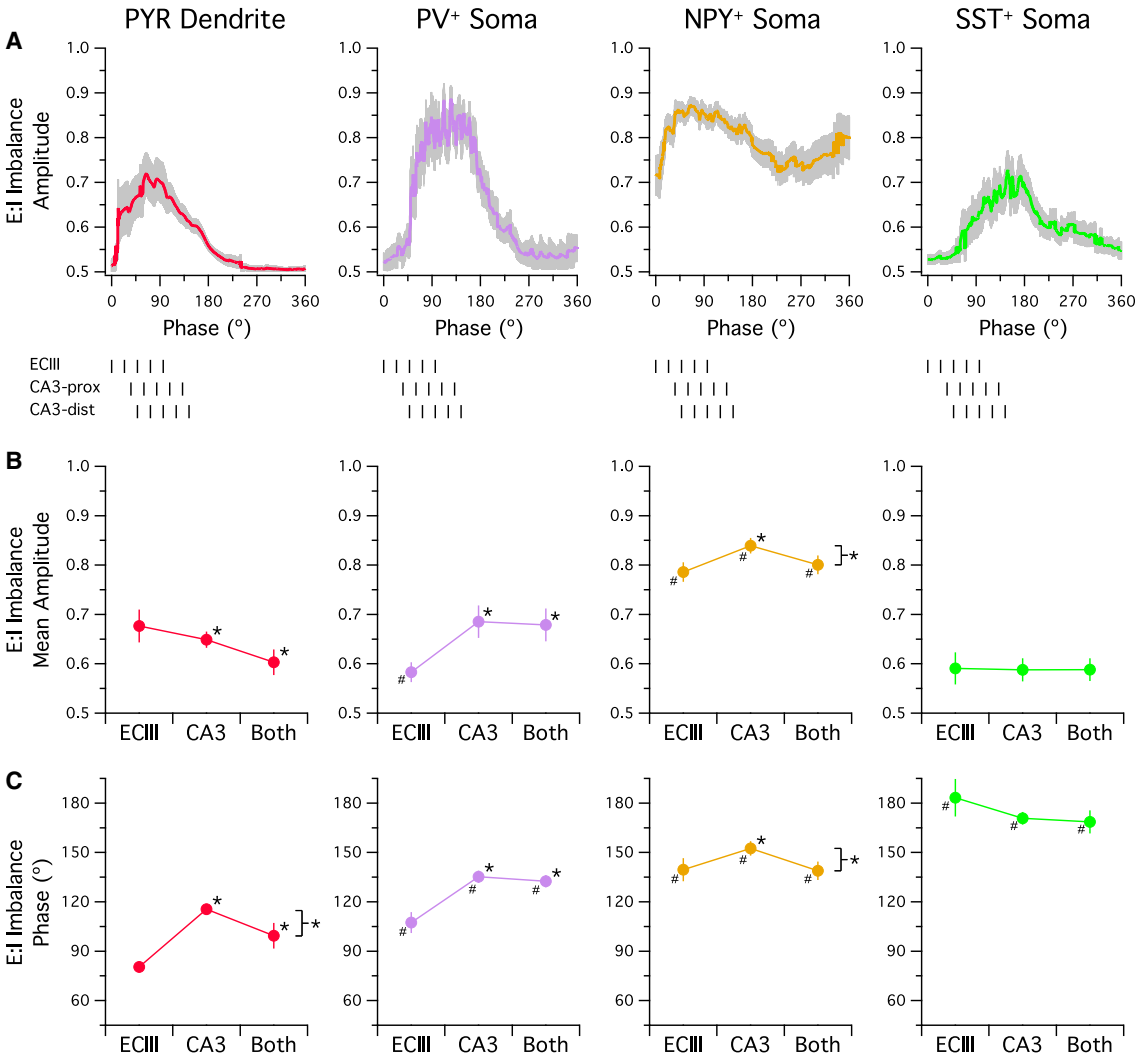

Figure 6. Dynamic Imbalance of Excitation and Inhibition in the CA1 Microcircuit

(A) Traces from the same pathway stimulation conditions and neuronal cell types as in Figures 2, 3, 4, and 5 were generated by offline removal of fast sodium spikes and hyperpolarizations below resting membrane potential, followed by linear interpolation to isolate the underlying depolarization waveforms. Then the measured depolarization waveforms from recordings with and without inhibition were used to calculate a continuous metric, "E:I Imbalance" (further described in Results and Experimental Procedures), so the relative contributions of the excitatory and inhibitory synaptic filters could be visualized and quantified. The resulting "E:I Imbalance" waveforms for each neuronal cell type are displayed here from recordings during co-stimulation of ECIII and CA3 input pathways. Solid lines represent the mean "E:I Imbalance" waveforms averaged across theta cycles and cells, and the gray shaded areas represent the SEM across cells. PYR (red): n = 11–18; PV^+ (purple): n = 8–10; NPY^+ (orange): n = 27–28; SST^+ (green): n = 11–15.

(B) The mean amplitude of "E:I Imbalance," quantified by averaging waveforms of the type shown in (A) across time, theta cycles, and cells, is displayed as mean ± SEM for each pathway stimulation condition and neuronal cell type. Floating asterisks denote a significant difference ($p < 0.05$) between the indicated pathway stimulation condition and ECIII inputs alone for the indicated cell type. Asterisks next to brackets denote a significant difference ($p < 0.05$) between CA3 inputs alone and both inputs together for the indicated cell type. Hash symbols denote a significant difference ($p < 0.05$) between the indicated cell type and pyramidal neurons (red) for the indicated pathway stimulation condition.

(C) Same as in (B) for the phase of "E:I Imbalance," averaged across theta cycles and cells. This is calculated from the center of mass of waveforms of the type shown in (A).

To determine which interneuron subpopulations are capable of mediating the inhibition of dendritic complex spiking shown in Figure 2, we next tested the functional impact of each interneuron class on dendritic excitability. We selectively activated specific subpopulations of interneurons by expressing the light-gated cation channel, channelrhodopsin-2 (ChR2), in a Cre recombinase-dependent manner. While the synaptically induced dendritic plateau potentials shown in Figure 2 were mediated partially by NMDA-Rs (Takahashi and Magee, 2009), we found that step current injections to the distal apical dendritic trunk region of pyramidal neurons were sufficient to induce periodic dendritic trunk spikes with a prolonged duration (Figure 7).

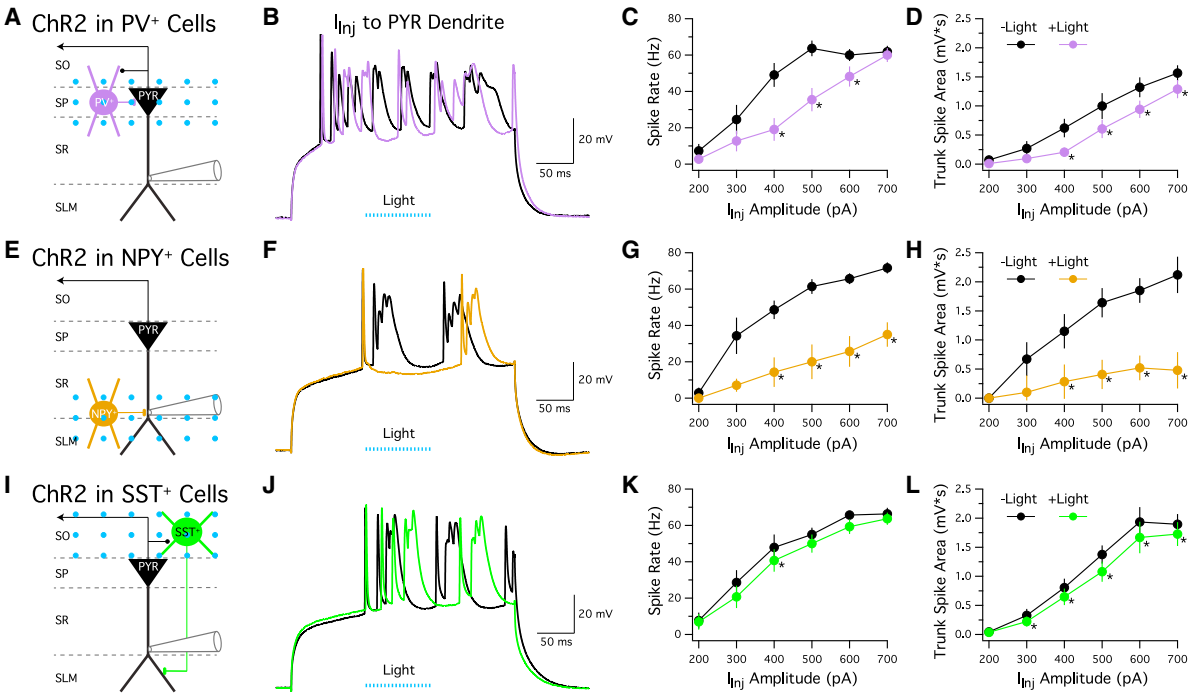

Figure 7. CA1 Interneuron Subtypes Differentially Gate Dendritic Excitability

(A) Schematic indicating recording position from the distal apical trunk dendrite of a CA1 pyramidal neuron near the border of SR and SLM (~300 μm from the cell body) during spatiotemporally patterned optical stimulation of ChR2 in PV^+ interneurons with a grid of light spots centered on SP.

(B) Example traces of a dendritic recording from a pyramidal neuron during a 300-ms-long step current injection (I_{Inj}) through the dendritic recording electrode with (purple) or without (black) optical stimulation of PV^+ interneurons, indicated by the blue dashes.

(C) The spike rate measured within a 100 ms window beginning at the start of optical stimulation, averaged across cells, is displayed as mean ± SEM for each I_{Inj} amplitude. Asterisks denote a significant difference ($p < 0.05$) between recordings with and without optical stimulation for the indicated I_{Inj} amplitude (n = 11).

(D) Same as (C) for the area of dendritic trunk spikes measured within a 100 ms window beginning at the start of optical stimulation, calculated as the area under the curve following offline removal of fast sodium spikes and linear interpolation, relative to the voltage threshold of the first spike per step I_{Inj}.

(E–H) Same as (A)–(D) for optical stimulation of NPY^+ interneurons with a grid of light spots centered on the border of SR and SLM (n = 6–7).

(I–L) Same as (A)–(D) for optical stimulation of SST^+ interneurons with a grid of light spots restricted to SO (n = 11–14).

See also Figures S1, S3, and S6.

These dendritic trunk spikes resembled those observed in neocortical layer 5 apical dendrites, which are mediated by voltage-gated Ca^{2+} channels and participate in the initiation of plateau potentials when combined with distal synaptic input (Harnett et al., 2013). We then measured inhibitory gating of these dendritic trunk spikes by pairing dendritic current injections with spatiotemporally patterned photoactivation of $ChR2^+$ interneurons with a collimated laser beam (schematized in Figure 7; see Experimental Procedures). We found that PV^+ interneuron activation with a grid of light spots centered on SP (Figure 7A) induced pauses in action potential firing in pyramidal cells (Figure 7B), reduced firing rates within a moderate range of injected current amplitudes (Figure 7C), and slightly reduced the area of dendritic trunk spikes (Figure 7D). These findings corroborate a recent report that inactivation of PV^+ interneurons in CA1 in vivo modulates the rate and timing of spiking in CA1 place cells (Royer et al., 2012).

Next we targeted SST^+ O-LM neurons by restricting photoactivation to SO (Figure 7I), resulting in a slight decrease in dendritic trunk spike area during the light stimulus (Figures 7J–7L). Similar results were also obtained by directly activating the terminals of O-LM axons in SLM (Figures S6D–S6F). This effect is of lesser magnitude than the reported effect of in vivo inactivation of SST^+ neurons on burst firing in CA1 place cells (Royer et al., 2012). This discrepancy is likely accounted for by the fact that O-LM inhibition is restricted to the distal dendritic tuft of pyramidal neurons, while our current injection was located in the apical trunk and lacked any synaptic NMDAR component; thus our measurement could underestimate the potency of O-LM inhibition on nonlinear integration of synaptic inputs in SLM.

Finally, we activated NPY^+ interneurons with light localized either to distal SR and SLM (Figure 7E) or restricted to SR (Figure S6A). In both cases we observed a dramatic reduction in simple and complex spiking in pyramidal neurons across a broad range of injected current amplitudes (Figures 7F–7H, S6B, and S6C). In many cases the induced inhibition completely aborted long duration trunk spikes for a period outlasting the duration of the light stimulus (Figure 7F), demonstrating that this subpopulation of CA1 interneurons provides a powerful gate for the amplification of dendritic signaling. A caveat is that, while the PV-Cre and SST-Cre mouse lines labeled interneurons that were ~97% restricted to SP and SO, the NPY-Cre line was

more heterogeneous, labeling not only interneurons at the SR/LM border, but also interneurons in other layers, including some O-LM neurons in SO and some putative neurogliaform cells in SLM (Figure S1) (Price et al., 2005; Somogyi and Klausberger, 2005). However, equivalent results were obtained whether or not the photoactivation area included SLM (Figures 7E–7H and S6A–S6C), arguing against a major contribution by neurons restricted to SLM. Furthermore, specific activation of a larger population of O-LM neurons in the SST-Cre line did not result in potent inhibition (Figures 7I–7L and S6D–S6F). Therefore, we attribute the distinct effect of ChR2 activation in NPY-Cre mice to neurons that contain processes in SR, including the SR/LM "border" interneurons characterized here (see example morphologies in Figure S2). Further refinement of genetic access to these interneuron subpopulations will be required to definitively determine their relative contributions to dendritic inhibition. These data provide functional relevance to the timing and firing rate information provided in Figures 4, 5, and 6 and suggest that the dual pathway integration observed in NPY^+ interneurons contributes to the suppression of dendritic plateau potentials and burst firing output from pyramidal neurons observed in Figures 2 and 3.

DISCUSSION

In this study we functionally dissected the network components of the local neuronal microcircuit in hippocampal area CA1 to understand the mechanisms that underlie nonlinear signal transformation and input feature selectivity. We found that synaptic inputs to this neuronal circuit layer encounter a series of spatiotemporal filters that select specific input patterns to be amplified and propagated as output to the next layer of the circuit. The first frequency-dependent filter encountered lies in presynaptic terminals, which exhibit differential short-term dynamics depending on the cell type of their postsynaptic target. Our results show that, at both proximal (CA3) and distal (ECIII) input pathways, inputs firing at low frequencies are attenuated by rapid-onset feedforward inhibition and summated sublinearly, while inputs firing in punctuated bursts are amplified by presynaptic facilitation and integrated supralinearly in dendrites. However, even input patterns that transiently unbalance excitation and inhibition in this manner and recruit pyramidal cells to spike are subject to additional inhibitory filtering that limits the mode and firing rate of output. We describe a source of feedforward inhibition to pyramidal dendrites that potently regulates dendritic complex spiking and suggest that feedback inhibition to distal dendrites first integrates facilitating output from pyramidal cells before providing a late-phase constraint on burst duration.

In the presence of these multiple components of inhibition, pyramidal cell firing rates were highest when coincident bursts at both ECIII and CA3 input pathways were rhythmically activated for multiple simulated theta cycles, demonstrating that slow changes in integration on the order of hundreds of milliseconds contribute to signal transformation in CA1. Under these conditions, we also observed advances in spike phase across theta cycles, another hallmark feature of CA1 place cells that occurs in vivo as an animal progresses through a cell's place field. While in our experiments, the rate and phase of presynaptic spikes remained constant across theta cycles, CA3 spikes in vivo exhibit increases in rate and advances in phase during place field traversal (Mizuseki et al., 2009, 2012). It is expected that such amplitude and phase modulation of inputs magnify these changes in CA1 (Losonczy et al., 2010; Chance, 2012), but our results suggest that mechanisms intrinsic to the CA1 microcircuit also contribute.

If inhibition in CA1 can so effectively predict and prevent supralinear integration in pyramidal cells, how are place cells able to exhibit robust spatially selective firing in vivo? A recent study of place cells in large environments reported that ~35% of CA1 pyramidal cells are silent in a ~50 m linear track (Rich et al., 2014). Of the remaining cells, ~95% contain between 1 and 13 place fields covering between 1% and 18% of the total length of the track (Rich et al., 2014). One possible explanation for this sparse coding is that each place cell fires in any and all locations where it receives strong excitatory input, but most cells do not receive excitatory inputs corresponding to ~82%–100% of locations in a given environment. However, Lee et al. (2012) recently demonstrated that place fields can be "awakened" in silent cells by somatic depolarization (see also Bittner et al., 2015). This indicates that place cells do receive a broader range of spatially tuned input than is revealed by their firing patterns. Our data support a prominent role for the inhibitory microcircuit in the selective gating of these spatially tuned inputs. Interestingly, recent studies inactivating either PV^+ (Atallah et al., 2012; Royer et al., 2012) or SST^+ (Royer et al., 2012) interneurons have reported changes in firing rate for cells within their receptive fields, a form of gain modulation, but not significant changes in stimulus selectivity or tuning. This raises the possibility that feedforward dendritic inhibitory mechanisms, including the NPY^+ "border" interneurons characterized in this study, contribute more specifically to the shaping of spatial receptive fields in the hippocampus. While earlier studies hinted at the physiological properties and functional impact of this class of interneurons (Lacaille and Schwartzkroin, 1988; Williams et al., 1994; Miles et al., 1996), the response properties and feature selectivity of these interneurons in vivo are completely unknown. Interestingly, a role for distal inhibition in gating distal dendritic regenerativity has also been observed in layer 5 pyramidal neurons in cortex (Larkum et al., 1999; Palmer et al., 2012), suggesting this may be a common feature of neuronal microcircuits in general.

While in this study we focused on three genetically defined subpopulations of CA1 interneurons, previous work has established prominent roles for additional inhibitory cell types not included in our analysis. In particular, a diverse class of interneurons expressing cholecystokinin (CCK) represent another source of feedforward dendritic inhibition (Megías et al., 2001; Klausberger, 2009; Basu et al., 2013). A recent thorough meta-analysis of anatomical data (Bezaire and Soltesz, 2013) estimated that PV^+, SST^+, CCK^+, neurogliaform, and NPY^+ "ivy" neurons (Lapray et al., 2012) account for ~56% of the interneurons and ~58% of the GABAergic synapses onto pyramidal dendrites. These sources likely contribute to the feedforward inhibition observed in our study in response to single pathway stimulation (Figures 1, 2, and 3). However, up to 40% of inhibitory boutons

onto pyramidal dendrites remain unclassified (Bezaire and Soltesz, 2013), and it is possible that the NPY$^+$ interneurons at the SR/SLM border characterized here fall into this category. Also expected to contribute critically to signal integration are the diverse actions of neuromodulators such as acetylcholine and serotonin on excitability and synaptic dynamics of both pyramidal neurons and interneurons in CA1 (Varga et al., 2009; Cea-del Rio et al., 2011).

Recent intracellular studies of hippocampal place cells have reported complex spikes to occur in vivo (Harvey et al., 2009; Epsztein et al., 2011; Grienberger et al., 2014; Bittner et al., 2015). Such events are estimated to account for 12.6% of all spikes emitted by place cells within their place fields (Epsztein et al., 2011). This relative sparsity is consistent with our finding that, even when pyramidal neurons receive spatiotemporal patterns of activity across both proximal and distal input pathways ideally suited for driving complex spikes, a feedforward inhibitory component of the circuit simultaneously responds to those same spatiotemporal correlations and decreases the responsiveness of pyramidal cells, a form of predictive coding (Srinivasan et al., 1982). Promising mechanisms to account for epochs of increased complex spike probability include neuromodulation (Hoffman and Johnston, 1999), disinhibition (Pi et al., 2013), and heterogeneity in the fine spatial structure of synaptic inputs (Druckmann et al., 2014).

EXPERIMENTAL PROCEDURES

All experiments and procedures were performed following protocols consistent with U.S. National Institute for Health guidelines and approved by the Institutional Animal Care and Use Committee at Janelia Research Campus, HHMI.

Hippocampal Slice Recordings

For recordings from CA1 pyramidal neuron dendrites, longitudinal slices of the hippocampus were prepared from 8- to 12-week-old rats (see Supplemental Experimental Procedures for detailed methods). Experiments involving targeted recordings or optical stimulation of genetically defined inhibitory interneurons were performed in slices from hemizygous knockin mice expressing Cre under the control of the endogenous promoters for PV (Hippenmeyer et al., 2005) (Jackson Laboratory), NPY (see Figure S8 and Supplemental Experimental Procedures), or SST (Lovett-Barron et al., 2012; Royer et al., 2012) (see Figures S1 and S2), crossed either to C57BL/6 (Charles River Laboratories) or Ai9 tdTomato reporter mice (Madisen et al., 2010) (Jackson Laboratory). For targeted patching of fluorescent interneurons, a brief two-photon frame scan was used to simultaneously acquire a digital image of emitted fluorescence as well as a digital Dodt gradient contrast image using a sub-stage detector. These images were then used as a reference to visualize and patch target cells using a traditional analog camera and Köhler illumination.

Cell Type-Specific Photoactivation

A recombinant adeno-associated virus (rAAV2/7) supporting Cre-dependent expression of ChR2-sfGFP (Figures 7 and S6) (Losonczy et al., 2010) was used for the selective photoactivation of CA1 interneurons (see Supplemental Experimental Procedures). A 473 nm continuous wave laser (Photonic Solutions) with a rapid internal modulation circuit was used to control the power, timing, and pulse duration (2 ms) of optical stimuli. Blue light was passed through collimating lens prior to a 20X (NA 1.0) objective (Carl Zeiss), resulting in ~100 μW light power with a columnar beam geometry ~20 μm in diameter at the surface of the tissue. Using a galvanometer-based scanning system (Prairie Technologies), the position of the spot was moved every 5 ms in random order to positions within a 3 × 6 rectangular grid, spaced at ~75 × ~125 μm intervals. Light power sufficient for photoactivation of CA1 interneurons expressing ChR2 was calibrated by recording from interneurons in slices from VGAT-Cre mice (Vong et al., 2011) (Jackson Laboratory), which resulted in spike rates for interneurons in SP (36.5 ± 24.0 Hz, n = 6), the SR/SLM border (20.1 ± 15.1 Hz, n = 4), and SO (90.1 ± 23.1 Hz, n = 3) that were comparable to those seen in response to electrical stimulation (Figures S6G–S6I).

Data Analysis

Voltage recordings were analyzed with custom scripts written in Igor Pro (Wavemetrics) (see Supplemental Experimental Procedures for details). In quantifying nonlinear input summation (Figures 1, 3, 5, and S5), we sought to characterize the transformation from spatiotemporal pattern of presynaptic spikes to postsynaptic depolarization, which included contributions from both presynaptic release dynamics and postsynaptic dendritic excitability. We used the average responses to low-frequency stimulation of single input pathways, when release terminals are in their basal state, to calculate the responses expected from linear temporal and spatial summation during theta burst stimulation. These expected depolarization waveforms were subtracted from measured depolarization waveforms to generate the traces shown and quantified in Figures 3 and 5. Within this framework, the response of a cell to high-frequency stimulation of multiple pathways would be equal to the expected linear sum if (1) presynaptic release probabilities were static and constant, and (2) spatial and temporal summation in the postsynaptic cell were linear. This method of analysis permits a straightforward interpretation of the effect of inhibition on the transfer function from presynaptic spikes to postsynaptic voltage, as well as direct comparison of the potency of inhibition during stimulation of individual pathways to that during dual pathway stimulation.

To quantify the dynamic interaction between excitation and inhibition, "E:I Imbalance" waveforms (Figure 6) were calculated by the equation E / (E + I), where E is the depolarization waveform measured in the absence of inhibition and I is the difference between the depolarization waveforms measured in the presence and absence of inhibition. This metric was only assigned a value for time points when (E + I) was greater than 2 mV. "Phase" of supralinear summation and "E:I Imbalance" was calculated from the center of mass of the waveform, or the point in time that divides the area under the curve in exactly half, for each theta cycle.

Statistics

All statistical modeling and hypothesis testing was performed using the open source software for statistical computing, "R" (R Core Team, 2013). We chose linear mixed effects modeling as a statistical framework that tolerates multiparametric paired experimental designs (Pinheiro and Bates, 2000) (see Supplemental Experimental Procedures for details). Wald F-tests were performed to determine the significance of the relationships between measured parameters (e.g., spike rate) and experimental factors (e.g., stimulation pathway). Post-hoc z-tests were performed to determine the significance of differences between levels of the examined factor (e.g., differences between specific stimulation pathway conditions). To account for multiple comparisons, p values were adjusted for false discovery rate (FDR) (Benjamini and Hochberg, 1995), and all comparisons with corrected p values < 0.05 were considered to be statistically significant (see Supplemental Statistics Tables).

SUPPLEMENTAL INFORMATION

Supplemental Information includes Supplemental Experimental Procedures, Supplemental Statistics Tables, and eight figures and can be found with this article online at http://dx.doi.org/10.1016/j.neuron.2015.08.025.

ACKNOWLEDGMENTS

We thank Bertalan Andrásfalvy for critical technical advice, training, and preliminary data early in the project and members of the Magee, Lee, Spruston, and Pastalkova labs for invaluable discussions.

Received: December 7, 2014
Revised: April 9, 2015
Accepted: August 14, 2015
Published: September 23, 2015

REFERENCES

Abbott, L.F., and Regehr, W.G. (2004). Synaptic computation. Nature *431*, 796–803.

Ahmed, O.J., and Mehta, M.R. (2009). The hippocampal rate code: anatomy, physiology and theory. Trends Neurosci. *32*, 329–338.

Ali, A.B., and Thomson, A.M. (1998). Facilitating pyramid to horizontal oriens-alveus interneurone inputs: dual intracellular recordings in slices of rat hippocampus. J. Physiol. *507*, 185–199.

Ang, C.W., Carlson, G.C., and Coulter, D.A. (2005). Hippocampal CA1 circuitry dynamically gates direct cortical inputs preferentially at theta frequencies. J. Neurosci. *25*, 9567–9580.

Atallah, B.V., and Scanziani, M. (2009). Instantaneous modulation of gamma oscillation frequency by balancing excitation with inhibition. Neuron *62*, 566–577.

Atallah, B.V., Bruns, W., Carandini, M., and Scanziani, M. (2012). Parvalbumin-expressing interneurons linearly transform cortical responses to visual stimuli. Neuron *73*, 159–170.

Bargmann, C.I., and Marder, E. (2013). From the connectome to brain function. Nat. Methods *10*, 483–490.

Basu, J., Srinivas, K.V., Cheung, S.K., Taniguchi, H., Huang, Z.J., and Siegelbaum, S.A. (2013). A cortico-hippocampal learning rule shapes inhibitory microcircuit activity to enhance hippocampal information flow. Neuron *79*, 1208–1221.

Benjamini, Y., and Hochberg, Y. (1995). Controlling the False Discovery Rate: A Practical and Powerful Approach to Multiple Testing. Journal of the Royal Statistical Society. Series B (Methodological) *57*, 289–300.

Bezaire, M.J., and Soltesz, I. (2013). Quantitative assessment of CA1 local circuits: knowledge base for interneuron-pyramidal cell connectivity. Hippocampus *23*, 751–785.

Bittner, K.C., Grienberger, C., Vaidya, S.P., Milstein, A.D., Macklin, J.J., Suh, J., Tonegawa, S., and Magee, J.C. (2015). Conjunctive input processing drives feature selectivity in hippocampal CA1 neurons. Nat. Neurosci. *18*, 1133–1142.

Bock, D.D., Lee, W.C., Kerlin, A.M., Andermann, M.L., Hood, G., Wetzel, A.W., Yurgenson, S., Soucy, E.R., Kim, H.S., and Reid, R.C. (2011). Network anatomy and in vivo physiology of visual cortical neurons. Nature *471*, 177–182.

Briggman, K.L., Helmstaedter, M., and Denk, W. (2011). Wiring specificity in the direction-selectivity circuit of the retina. Nature *471*, 183–188.

Brun, V.H., Otnass, M.K., Molden, S., Steffenach, H.-A., Witter, M.P., Moser, M.-B., and Moser, E.I. (2002). Place cells and place recognition maintained by direct entorhinal-hippocampal circuitry. Science *296*, 2243–2246.

Buzsáki, G. (2002). Theta oscillations in the hippocampus. Neuron *33*, 325–340.

Buzsáki, G., and Moser, E.I. (2013). Memory, navigation and theta rhythm in the hippocampal-entorhinal system. Nat. Neurosci. *16*, 130–138.

Cea-del Rio, C.A., Lawrence, J.J., Erdelyi, F., Szabo, G., and McBain, C.J. (2011). Cholinergic modulation amplifies the intrinsic oscillatory properties of CA1 hippocampal cholecystokinin-positive interneurons. J. Physiol. *589*, 609–627.

Chance, F.S. (2012). Hippocampal phase precession from dual input components. J. Neurosci. *32*, 16693–16703a.

Chevaleyre, V., and Siegelbaum, S.A. (2010). Strong CA2 pyramidal neuron synapses define a powerful disynaptic cortico-hippocampal loop. Neuron *66*, 560–572.

deCharms, R.C., and Zador, A. (2000). Neural representation and the cortical code. Annu. Rev. Neurosci. *23*, 613–647.

Druckmann, S., Feng, L., Lee, B., Yook, C., Zhao, T., Magee, J.C., and Kim, J. (2014). Structured synaptic connectivity between hippocampal regions. Neuron *81*, 629–640.

Eichenbaum, H. (2013). Memory on time. Trends Cogn. Sci. *17*, 81–88.

Epsztein, J., Brecht, M., and Lee, A.K. (2011). Intracellular determinants of hippocampal CA1 place and silent cell activity in a novel environment. Neuron *70*, 109–120.

George, A.A., Lyons-Warren, A.M., Ma, X., and Carlson, B.A. (2011). A diversity of synaptic filters are created by temporal summation of excitation and inhibition. J. Neurosci. *31*, 14721–14734.

Grienberger, C., Chen, X., and Konnerth, A. (2014). NMDA receptor-dependent multidendrite $Ca^{(2+)}$ spikes required for hippocampal burst firing in vivo. Neuron *81*, 1274–1281.

Grillner, S., Markram, H., De Schutter, E., Silberberg, G., and LeBeau, F.E. (2005). Microcircuits in action–from CPGs to neocortex. Trends Neurosci. *28*, 525–533.

Haider, B., Duque, A., Hasenstaub, A.R., and McCormick, D.A. (2006). Neocortical network activity in vivo is generated through a dynamic balance of excitation and inhibition. J. Neurosci. *26*, 4535–4545.

Harnett, M.T., Xu, N.L., Magee, J.C., and Williams, S.R. (2013). Potassium channels control the interaction between active dendritic integration compartments in layer 5 cortical pyramidal neurons. Neuron *79*, 516–529.

Harvey, C.D., Collman, F., Dombeck, D.A., and Tank, D.W. (2009). Intracellular dynamics of hippocampal place cells during virtual navigation. Nature *461*, 941–946.

Hippenmeyer, S., Vrieseling, E., Sigrist, M., Portmann, T., Laengle, C., Ladle, D.R., and Arber, S. (2005). A developmental switch in the response of DRG neurons to ETS transcription factor signaling. PLoS Biol. *3*, e159.

Hoffman, D.A., and Johnston, D. (1999). Neuromodulation of dendritic action potentials. J. Neurophysiol. *81*, 408–411.

Isaacson, J.S., and Scanziani, M. (2011). How inhibition shapes cortical activity. Neuron *72*, 231–243.

Johnston, D., Magee, J.C., Colbert, C.M., and Cristie, B.R. (1996). Active properties of neuronal dendrites. Annu. Rev. Neurosci. *19*, 165–186.

Jones, H.C., and Keep, R.F. (1988). Brain fluid calcium concentration and response to acute hypercalcaemia during development in the rat. J. Physiol. *402*, 579–593.

Kajiwara, R., Wouterlood, F.G., Sah, A., Boekel, A.J., Baks-te Bulte, L.T.G., and Witter, M.P. (2008). Convergence of entorhinal and CA3 inputs onto pyramidal neurons and interneurons in hippocampal area CA1–an anatomical study in the rat. Hippocampus *18*, 266–280.

Kim, J., Zhao, T., Petralia, R.S., Yu, Y., Peng, H., Myers, E., and Magee, J.C. (2012). mGRASP enables mapping mammalian synaptic connectivity with light microscopy. Nat. Methods *9*, 96–102.

Klausberger, T. (2009). GABAergic interneurons targeting dendrites of pyramidal cells in the CA1 area of the hippocampus. Eur. J. Neurosci. *30*, 947–957.

Klyachko, V.A., and Stevens, C.F. (2006). Excitatory and feed-forward inhibitory hippocampal synapses work synergistically as an adaptive filter of natural spike trains. PLoS Biol. *4*, e207.

Knowles, W.D., and Schwartzkroin, P.A. (1981). Local circuit synaptic interactions in hippocampal brain slices. J. Neurosci. *1*, 318–322.

Lacaille, J.C., and Schwartzkroin, P.A. (1988). Stratum lacunosum-moleculare interneurons of hippocampal CA1 region. I. Intracellular response characteristics, synaptic responses, and morphology. J. Neurosci. *8*, 1400–1410.

Lapray, D., Lasztóczi, B., Lagler, M., Viney, T.J., Katona, L., Valenti, O., Hartwich, K., Borhegyi, Z., Somogyi, P., and Klausberger, T. (2012). Behavior-dependent specialization of identified hippocampal interneurons. Nat. Neurosci. *15*, 1265–1271.

Larkum, M. (2013). A cellular mechanism for cortical associations: an organizing principle for the cerebral cortex. Trends Neurosci. *36*, 141–151.

Larkum, M.E., Zhu, J.J., and Sakmann, B. (1999). A new cellular mechanism for coupling inputs arriving at different cortical layers. Nature *398*, 338–341.

Lee, D., Lin, B.J., and Lee, A.K. (2012). Hippocampal place fields emerge upon single-cell manipulation of excitability during behavior. Science *337*, 849–853.

London, M., and Häusser, M. (2005). Dendritic computation. Annu. Rev. Neurosci. *28*, 503–532.

Losonczy, A., and Magee, J.C. (2006). Integrative properties of radial oblique dendrites in hippocampal CA1 pyramidal neurons. Neuron *50*, 291–307.

Losonczy, A., Zhang, L., Shigemoto, R., Somogyi, P., and Nusser, Z. (2002). Cell type dependence and variability in the short-term plasticity of EPSCs in identified mouse hippocampal interneurones. J. Physiol. *542*, 193–210.

Losonczy, A., Zemelman, B.V., Vaziri, A., and Magee, J.C. (2010). Network mechanisms of theta related neuronal activity in hippocampal CA1 pyramidal neurons. Nat. Neurosci. *13*, 967–972.

Lovett-Barron, M., Turi, G.F., Kaifosh, P., Lee, P.H., Bolze, F., Sun, X.-H., Nicoud, J.-F., Zemelman, B.V., Sternson, S.M., and Losonczy, A. (2012). Regulation of neuronal input transformations by tunable dendritic inhibition. Nat. Neurosci. *15*, 423–430, S1–S3.

Maccaferri, G., and McBain, C.J. (1995). Passive propagation of LTD to stratum oriens-alveus inhibitory neurons modulates the temporoammonic input to the hippocampal CA1 region. Neuron *15*, 137–145.

Madisen, L., Zwingman, T.A., Sunkin, S.M., Oh, S.W., Zariwala, H.A., Gu, H., Ng, L.L., Palmiter, R.D., Hawrylycz, M.J., Jones, A.R., et al. (2010). A robust and high-throughput Cre reporting and characterization system for the whole mouse brain. Nat. Neurosci. *13*, 133–140.

Magee, J.C. (2000). Dendritic integration of excitatory synaptic input. Nat. Rev. Neurosci. *1*, 181–190.

Magee, J.C., and Johnston, D. (1997). A synaptically controlled, associative signal for Hebbian plasticity in hippocampal neurons. Science *275*, 209–213.

Markram, H., Gupta, A., Uziel, A., Wang, Y., and Tsodyks, M. (1998). Information processing with frequency-dependent synaptic connections. Neurobiol. Learn. Mem. *70*, 101–112.

Megías, M., Emri, Z., Freund, T.F., and Gulyás, A.I. (2001). Total number and distribution of inhibitory and excitatory synapses on hippocampal CA1 pyramidal cells. Neuroscience *102*, 527–540.

Miles, R., Tóth, K., Gulyás, A.I., Hájos, N., and Freund, T.F. (1996). Differences between somatic and dendritic inhibition in the hippocampus. Neuron *16*, 815–823.

Mizuseki, K., Sirota, A., Pastalkova, E., and Buzsáki, G. (2009). Theta oscillations provide temporal windows for local circuit computation in the entorhinal-hippocampal loop. Neuron *64*, 267–280.

Mizuseki, K., Royer, S., Diba, K., and Buzsáki, G. (2012). Activity dynamics and behavioral correlates of CA3 and CA1 hippocampal pyramidal neurons. Hippocampus *22*, 1659–1680.

Mori, M., Abegg, M.H., Gähwiler, B.H., and Gerber, U. (2004). A frequency-dependent switch from inhibition to excitation in a hippocampal unitary circuit. Nature *431*, 453–456.

Murthy, V.N., Sejnowski, T.J., and Stevens, C.F. (1997). Heterogeneous release properties of visualized individual hippocampal synapses. Neuron *18*, 599–612.

Nakashiba, T., Young, J.Z., McHugh, T.J., Buhl, D.L., and Tonegawa, S. (2008). Transgenic inhibition of synaptic transmission reveals role of CA3 output in hippocampal learning. Science *319*, 1260–1264.

O'Keefe, J. (1979). A review of the hippocampal place cells. Prog. Neurobiol. *13*, 419–439.

Palmer, L.M., Schulz, J.M., Murphy, S.C., Ledergerber, D., Murayama, M., and Larkum, M.E. (2012). The cellular basis of GABA(B)-mediated interhemispheric inhibition. Science *335*, 989–993.

Petreanu, L., Mao, T., Sternson, S.M., and Svoboda, K. (2009). The subcellular organization of neocortical excitatory connections. Nature *457*, 1142–1145.

Pfeffer, C.K., Xue, M., He, M., Huang, Z.J., and Scanziani, M. (2013). Inhibition of inhibition in visual cortex: the logic of connections between molecularly distinct interneurons. Nat. Neurosci. *16*, 1068–1076.

Pi, H.J., Hangya, B., Kvitsiani, D., Sanders, J.I., Huang, Z.J., and Kepecs, A. (2013). Cortical interneurons that specialize in disinhibitory control. Nature *503*, 521–524.

Pinheiro, J., and Bates, D. (2000). Mixed-effects models in S and S-PLUS (New York: Springer).

Pouille, F., and Scanziani, M. (2001). Enforcement of temporal fidelity in pyramidal cells by somatic feed-forward inhibition. Science *293*, 1159–1163.

Pouille, F., and Scanziani, M. (2004). Routing of spike series by dynamic circuits in the hippocampus. Nature *429*, 717–723.

Price, C.J., Cauli, B., Kovacs, E.R., Kulik, A., Lambolez, B., Shigemoto, R., and Capogna, M. (2005). Neurogliaform neurons form a novel inhibitory network in the hippocampal CA1 area. J. Neurosci. *25*, 6775–6786.

R Core Team (2013). R: A language and environment for statistical computing (Vienna, Austria: R Foundation for Statistical Computing).

Reyes, A., Lujan, R., Rozov, A., Burnashev, N., Somogyi, P., and Sakmann, B. (1998). Target-cell-specific facilitation and depression in neocortical circuits. Nat. Neurosci. *1*, 279–285.

Rich, P.D., Liaw, H.P., and Lee, A.K. (2014). Place cells. Large environments reveal the statistical structure governing hippocampal representations. Science *345*, 814–817.

Richardson, M.J., Melamed, O., Silberberg, G., Gerstner, W., and Markram, H. (2005). Short-term synaptic plasticity orchestrates the response of pyramidal cells and interneurons to population bursts. J. Comput. Neurosci. *18*, 323–331.

Royer, S., Zemelman, B.V., Losonczy, A., Kim, J., Chance, F., Magee, J.C., and Buzsáki, G. (2012). Control of timing, rate and bursts of hippocampal place cells by dendritic and somatic inhibition. Nat. Neurosci. *15*, 769–775.

Schomburg, E.W., Fernández-Ruiz, A., Mizuseki, K., Berényi, A., Anastassiou, C.A., Koch, C., and Buzsáki, G. (2014). Theta phase segregation of input-specific gamma patterns in entorhinal-hippocampal networks. Neuron *84*, 470–485.

Silberberg, G., Grillner, S., LeBeau, F.E., Maex, R., and Markram, H. (2005). Synaptic pathways in neural microcircuits. Trends Neurosci. *28*, 541–551.

Somogyi, P., and Klausberger, T. (2005). Defined types of cortical interneurone structure space and spike timing in the hippocampus. J. Physiol. *562*, 9–26.

Somogyi, P., Katona, L., Klausberger, T., Lasztóczi, B., and Viney, T.J. (2014). Temporal redistribution of inhibition over neuronal subcellular domains underlies state-dependent rhythmic change of excitability in the hippocampus. Philos. Trans. R. Soc. Lond. B Biol. Sci. *369*, 20120518.

Spruston, N. (2008). Pyramidal neurons: dendritic structure and synaptic integration. Nat. Rev. Neurosci. *9*, 206–221.

Srinivasan, M.V., Laughlin, S.B., and Dubs, A. (1982). Predictive coding: a fresh view of inhibition in the retina. Proc. R. Soc. Lond. B Biol. Sci. *216*, 427–459.

Sun, H.Y., Lyons, S.A., and Dobrunz, L.E. (2005). Mechanisms of target-cell specific short-term plasticity at Schaffer collateral synapses onto interneurones versus pyramidal cells in juvenile rats. J. Physiol. *568*, 815–840.

Takács, V.T., Klausberger, T., Somogyi, P., Freund, T.F., and Gulyás, A.I. (2012). Extrinsic and local glutamatergic inputs of the rat hippocampal CA1 area differentially innervate pyramidal cells and interneurons. Hippocampus *22*, 1379–1391.

Takahashi, H., and Magee, J.C. (2009). Pathway interactions and synaptic plasticity in the dendritic tuft regions of CA1 pyramidal neurons. Neuron *62*, 102–111.

Varga, V., Losonczy, A., Zemelman, B.V., Borhegyi, Z., Nyiri, G., Domonkos, A., Hangya, B., Holderith, N., Magee, J.C., and Freund, T.F. (2009). Fast synaptic subcortical control of hippocampal circuits. Science *326*, 449–453.

Vong, L., Ye, C., Yang, Z., Choi, B., Chua, S., Jr., and Lowell, B.B. (2011). Leptin action on GABAergic neurons prevents obesity and reduces inhibitory tone to POMC neurons. Neuron *71*, 142–154.

Wierenga, C.J., and Wadman, W.J. (2003). Excitatory inputs to CA1 interneurons show selective synaptic dynamics. J. Neurophysiol. *90*, 811–821.

Williams, S., Samulack, D.D., Beaulieu, C., and LaCaille, J.-C. (1994). Membrane properties and synaptic responses of interneurons located near the stratum lacunosum-moleculare/radiatum border of area CA1 in whole-cell recordings from rat hippocampal slices. J. Neurophysiol. *71*, 2217–2235.

Witter, M.P. (1993). Organization of the entorhinal-hippocampal system: a review of current anatomical data. Hippocampus *3*, 33–44.

Womelsdorf, T., Valiante, T.A., Sahin, N.T., Miller, K.J., and Tiesinga, P. (2014). Dynamic circuit motifs underlying rhythmic gain control, gating and integration. Nat. Neurosci. *17*, 1031–1039.

Xu, N.L., Harnett, M.T., Williams, S.R., Huber, D., O'Connor, D.H., Svoboda, K., and Magee, J.C. (2012). Nonlinear dendritic integration of sensory and motor input during an active sensing task. Nature *492*, 247–251.

Xue, M., Atallah, B.V., and Scanziani, M. (2014). Equalizing excitation-inhibition ratios across visual cortical neurons. Nature *511*, 596–600.